Commun. Comput. Phys.
doi: 10.4208/cicp.301009.161210s

Vol. **9**, No. 5, pp. 1335-1346
May 2011

Gas Transport Properties in Gas Diffusion Layers: A Lattice Boltzmann Study

Toshihisa Munekata[1,2,*], Takaji Inamuro[2,3] and Shi-aki Hyodo[1]

[1] *Materials Design Laboratory, Toyota Central R&D Labs., Inc., Nagakute, Aichi 480-1192, Japan.*
[2] *Department of Aeronautics and Astronautics, Graduate School of Engineering, Kyoto University, Kyoto 606-8501, Japan.*
[3] *Advanced Research Institute of Fluid Science and Engineering, Graduate School of Engineering, Kyoto University, Kyoto 606-8501, Japan.*

Received 30 October 2009; Accepted (in revised version) 16 December 2010

Available online 18 February 2011

Abstract. The lattice Boltzmann method is applied to the investigations of the diffusivity and the permeability in the gas diffusion layer (GDL) of the polymer electrolyte fuel cell (PEFC). The effects of the configuration of water droplets, the porosity of the GDL, the viscosity ratio of water to air, and the surface wettability of the GDL are investigated. From the simulations under the PEFC operating conditions, it is found that the heterogeneous water network and the high porosity improve the diffusivity and the permeability, and the hydrophobic surface decreases the permeability.

AMS subject classifications: 76S05, 76R50, 76R05, 76M28

Key words: Diffusivity, permeability, lattice Boltzmann method, gas diffusion layer.

1 Introduction

Polymer electrolyte fuel cells (PEFCs) are expected as one of the alternative energy sources. The management of generated water in the PEFC is important especially at the cathode side, since the generated water prevents oxygen from reaching a catalyst layer. In order to remove the generated water from the catalyst layer and provide the continuous transport of oxygen, gas diffusion layers (GDLs) are bound with the catalyst layer. Therefore, the understanding and the improvement of drainage and gas transport properties in the GDL are important issues to realize the high performance of the PEFC [1].

In this study, we focus on the gas transport in the GDL. Among the gas transport properties, we consider the diffusivity (Fick's law) [2] and the permeability (Darcy's

*Corresponding author. *Email addresses:* munekata@mosk.tytlabs.co.jp (T. Munekata), inamuro@kuaero.kyoto-u.ac.jp (T. Inamuro), e0668@mosk.tytlabs.co.jp (S. Hyodo)

law) [3]. These properties have been roughly estimated by simple models or by empirical rules [4], but in those works the PEFC operating conditions such as the water network, the viscosity ratio of water to air, and the surface wettability of the GDL are neglected. However, these conditions may affect the gas transport properties. So, we investigate the effects of the PEFC operating conditions on the diffusivity and the permeability of the GDL by using the lattice Boltzmann method (LBM). In recent years, the LBM has succeeded in simulating flows in porous media, because of the simple algorithm without convergent calculations and the easy handling of local boundary conditions.

The outline of this paper is the following. In Section 2, the problem is described. In Section 3, the numerical method is presented. In Section 4, the numerical simulations are carried out to investigate the effects of droplet configuration, structure porosity, viscosity ratio of water to air, and surface wettability. Conclusions are given in Section 5.

2 Problem setting

The whole calculation process is divided into two steps. First, the equilibrium configuration of water droplets in the gas diffusion layer (GDL) is made up. Next, the diffusivity and the permeability in the GDL containing water droplets are examined.

2.1 GDL structure and water configuration

In this study, a GDL structure is constructed by randomly laminated fibers as shown in Fig. 1. The whole domain is discretized into 101^3 grid points, and its resolution is 4×10^{-6}m. The diameter of the fiber is 3 grids, and 700 fibers are placed in the structure.

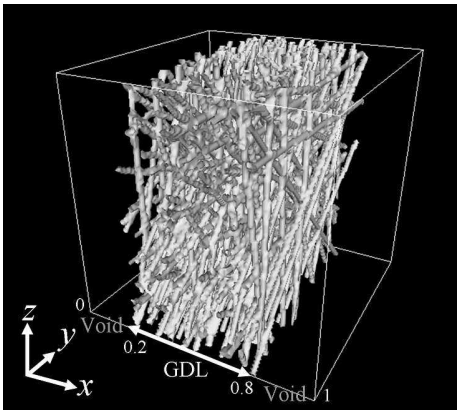

Figure 1: A GDL used in the simulations. Gray and transparent area are for solid and fluid spaces, respectively.

In the operating PEFC, the GDL pores are partly filled with the generated water. So the water configuration is modelled by droplets. The water droplets are placed randomly in the GDL as the initial configuration (Fig. 2(a)). The size of droplets is also chosen at

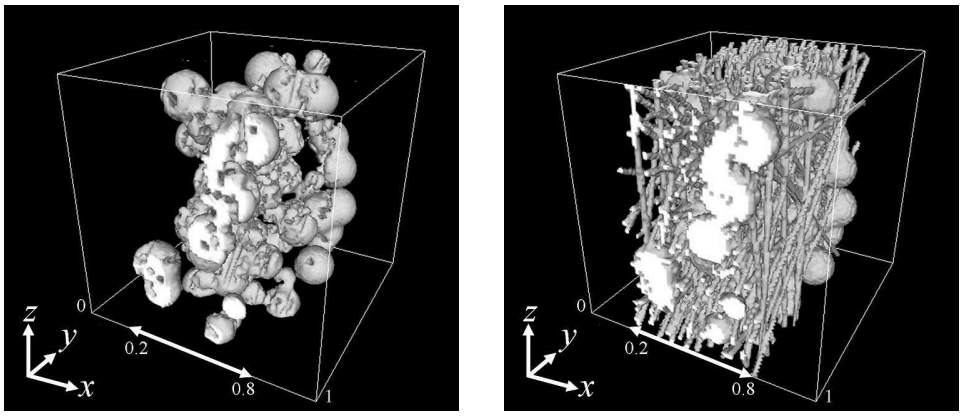

(a) (b)

Figure 2: (a) Random droplets of water (initial configuration), and (b) fibers and droplets.

random. Then the equilibrium configuration of water droplets is calculated by using the two-phase LBM model [5–7]. By combining the above two structures of fibers and droplets, we make a mimic GDL in the operating PEFC (Fig. 2(b)).

The equilibrium configuration of water droplets is affected by the operating conditions. Among various operating parameters, we select the droplet radius (R), the porosity of the GDL (ϵ), the viscosity ratio ($M = \mu_{\text{water}}/\mu_{\text{air}}$), the wettability of the GDL surface (contact angle θ), and the water saturation in the GDL ($S_{\text{w}} =$ volume of water/volume of pores). By changing these parameters, we make the equilibrium configuration of water droplets. The calculation conditions are listed in Table 1. Set 1 is the standard condition. The radius is in the range of 16 to 24μm, the porosity is 80%, the viscosity ratio is 50 (25°C), and the neutral wettability (90°) is selected. For Set 2, the range of droplet radius is changed to 16 to 40μm. By this change, the effect of the nonuniform size of water droplets is examined. For Sets 3 and 4, the porosity is changed from 80% to 75 and 86%. For Sets 5 and 6, the viscosity ratio is changed from 50 (25°C) to 15 (90°C) and 100 (0°C), in order to investigate the effect of the viscosity ratio that relates

Table 1: Calculation conditions for the equilibrium configuration of water droplets.

Calculation Condition	Water saturation $S_{\text{w}}/\%$	Droplet radius $R/\mu m$	Porosity $\epsilon/\%$	Viscosity ratio M/-	Wettability (Contact angle θ)
Set 1	$0 \sim 70$	$16 \sim 24$	80	50 (25°C)	Neutral (90°)
Set 2	$0 \sim 70$	$16 \sim 40$	80	50 (25°C)	Neutral (90°)
Set 3	$0 \sim 60$	$16 \sim 24$	75	50 (25°C)	Neutral (90°)
Set 4	$0 \sim 60$	$16 \sim 24$	86	50 (25°C)	Neutral (90°)
Set 5	$0 \sim 60$	$16 \sim 24$	80	15 (90°C)	Neutral (90°)
Set 6	$0 \sim 60$	$16 \sim 24$	80	100 (0°C)	Neutral (90°)
Set 7	$0 \sim 60$	$16 \sim 24$	80	50 (25°C)	Hydrophobic (120°)
Set 8	$0 \sim 60$	$16 \sim 24$	80	50 (25°C)	Hydrophobic (150°)

the operating temperature. For Sets 7 and 8, the wettability is changed from neutral (90°) to hydrophobic (120° and 150°). For each Set, we treat the water saturation as a main parameter, because this parameter is dynamically changed in the operating PEFC.

2.2 Gas transport properties

In the above mimic GDL, we consider the oxygen diffusivity and the air permeability. The relative diffusivity [2, 4] is defined as follows:

$$D_{\rm r}=\frac{F(S_{\rm w},R,\epsilon,M,\theta)}{F(S_{\rm w}=0\%,R=0,\epsilon=100\%,M=50,\theta=90^\circ)}, \tag{2.1}$$

where F is the total mass flow by diffusion.

The dimensionless permeability [3] is defined as follows:

$$K_{\rm dl}=\frac{\mu|U_{\rm average}(S_{\rm w},R,\epsilon,M,\theta)|}{L\Delta P}, \tag{2.2}$$

where μ is the viscosity coefficient, $U_{\rm average}$ is the volume averaged velocity, L is the thickness of the GDL, and ΔP is the pressure difference between L.

These values depend on the structure of fibers and droplets and are independent of the gas species [10]. Obviously the large values are desirable for the gas supply.

3 Method

3.1 Governing equations

For the simulations of diffusion in the mimic GDL, we use the diffusion equation:

$$\frac{\partial C}{\partial t}=D\nabla^2 C, \tag{3.1}$$

where C is the oxygen concentration, t is the time, and D is the diffusion coefficient.

For the simulations of gas flows in the mimic GDL, the incompressible Navier-Stokes equation is employed.

$$\nabla\boldsymbol{u}=0,\qquad \frac{\partial\boldsymbol{u}}{\partial t}+(\boldsymbol{u}\cdot\nabla)\boldsymbol{u}=-\frac{1}{\rho}\nabla p+\frac{\mu}{\rho}\nabla^2\boldsymbol{u}, \tag{3.2}$$

where $\boldsymbol{u}$ is the velocity, ρ is the air density, p is the pressure, and μ is the viscosity.

On the surfaces of the fibers and the water droplets in the GDL, it is assumed that both the oxygen and the air satisfy no permeable and no slip condition, because the gas permeability to the fibers and the gas solubility in water are negligibly small.

3.2 Lattice Boltzmann method

To solve the above Eqs. (3.1) and (3.2), we use the lattice Boltzmann method (LBM). In the LBM, the time and space evolution of the distribution function f_i is computed by

$$f_i(\boldsymbol{x}+\boldsymbol{c}_i\delta t,t+\delta t)-f_i(\boldsymbol{x},t)=-T^{-1}ST\left[f_i(\boldsymbol{x},t)-f_i^{\rm eq}(\boldsymbol{x},t)\right], \tag{3.3}$$

where $\boldsymbol{x}$ is the position, $\boldsymbol{c}_i$ is the particle velocity, t is the time, δt is the time increment, T is the transformation matrix, S is the multiple-relaxation-time, and $f_i^{\rm eq}$ is the equilibrium distribution function. Here D3Q19 ($i=0\sim18$) model is used for the particle velocity $\boldsymbol{c}_i$:

$$\begin{aligned}&\left[\boldsymbol{c}_0,\boldsymbol{c}_1,\boldsymbol{c}_2,\boldsymbol{c}_3,\boldsymbol{c}_4,\boldsymbol{c}_5,\boldsymbol{c}_6,\boldsymbol{c}_7,\boldsymbol{c}_8,\boldsymbol{c}_9,\boldsymbol{c}_{10},\boldsymbol{c}_{11},\boldsymbol{c}_{12},\boldsymbol{c}_{13},\boldsymbol{c}_{14},\boldsymbol{c}_{15},\boldsymbol{c}_{16},\boldsymbol{c}_{17},\boldsymbol{c}_{18}\right]\\ &=\begin{bmatrix} 0 & 1 & -1 & 0 & 0 & 0 & 0 & 1 & -1 & 1 & -1 & 1 & -1 & 1 & -1 & 0 & 0 & 0 & 0\\ 0 & 0 & 0 & 1 & -1 & 0 & 0 & 1 & -1 & -1 & 1 & 0 & 0 & 0 & 0 & 1 & -1 & 1 & -1\\ 0 & 0 & 0 & 0 & 0 & 1 & -1 & 0 & 0 & 0 & 0 & 1 & -1 & -1 & 1 & 1 & -1 & -1 & 1 \end{bmatrix}.\end{aligned} \tag{3.4}$$

In order to enhance the accuracy and the stability of the scheme, the multiple-relaxation-time (MRT) scheme $T^{-1}ST$ [3, 11, 12] is adopted. The multiple-relaxation-time is as follows:

$$S_{0,1,2,3,5,7,9,10,11,12,13,14,15}=\frac{1}{\tau},\qquad S_{4,6,8,16,17,18}=8\frac{2\tau-1}{8\tau-1}, \tag{3.5}$$

where τ is the relaxation time.

3.2.1 Diffusion model

For the computation of Eq. (3.1), the diffusion model [2] is employed.

$$f_i^{\rm eq}=w_iC,\qquad C=\sum_{i=0}^{18}f_i, \tag{3.6a}$$

$$D=\frac{2\tau-1}{6},\qquad w_i=\begin{cases}\frac{1}{3}, & i=0,\\ \frac{1}{18}, & i=1\sim6,\\ \frac{1}{36}, & i=7\sim18,\end{cases} \tag{3.6b}$$

where w_i is the weight coefficient. The diffusion flux N_α is calculated by

$$N_\alpha=\sum_{i=1}^{18}c_{i\alpha}f_i, \tag{3.7}$$

with subscripts $\alpha,\beta,\gamma=x,y,z$. The total mass flow F in Eq. (2.1) is calculated from an area integral of the diffusion flux N_α.

3.2.2 Incompressible model

For the computation of Eq. (3.2), the incompressible model [13] is employed.

$$f_i^{\rm eq}=w_i\left[3p+3c_{i\alpha}u_\alpha+\frac{9}{2}c_{i\alpha}c_{i\beta}u_\alpha u_\beta-\frac{3}{2}u_\alpha^2\right], \tag{3.8a}$$

$$3p=\sum_{i=0}^{18}f_i,\qquad u_\alpha=\sum_{i=1}^{18}c_{i\alpha}f_i,\qquad \frac{\mu}{\rho}=\frac{2\tau-1}{6}. \tag{3.8b}$$

The volume averaged velocity U_{average} in Eq. (2.2) is calculated from a volume average of the velocity u_α in the whole domain.

3.2.3 Boundary condition

On the surfaces of the fibers and the droplets, the halfway bounce back boundary condition [14] is used. The combination of the MRT scheme and the halfway bounce back boundary condition enables to implement the no permeable boundary condition for the diffusion equation (3.1) and the no slip boundary condition for the Navier-Stokes equation (3.2) on the complex geometry [12]. On the y-z plane, the concentration difference boundary condition [16] is used as shown Fig. 3(a) for the diffusivity, and the pressure difference boundary condition [15] is used as shown Fig. 3(b) for the permeability. On the x-y and x-z planes, the periodic boundary condition is implemented.

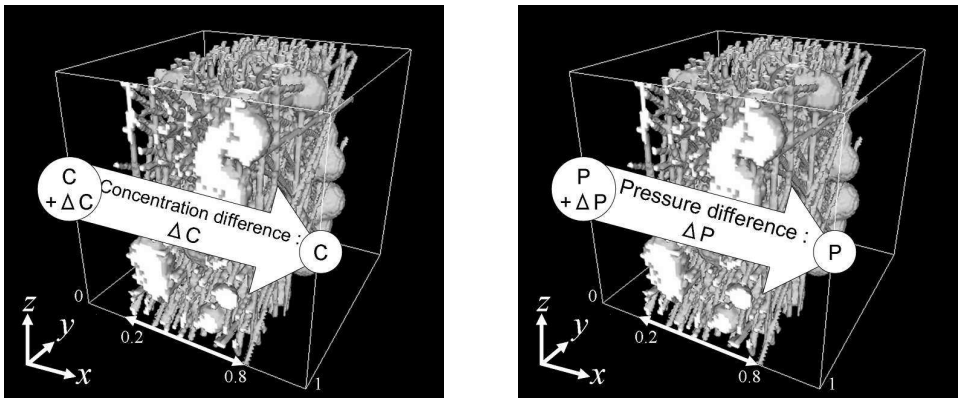

(a) (b)

Figure 3: Calculation setup for (a) the diffusivity and for (b) the permeability.

4 Results and discussion

The effect of the operating conditions (Table 1) on the gas transport properties is examined. We make five different initial configurations of water droplets for each condition, and the averaged values of the water saturation, the diffusivity and the permeability over the five different mimic GDL are shown in the following figures.

4.1 The effect of heterogeneous configuration of water droplets (Sets 1 and 2)

Fig. 4 shows the configuration of water droplets for Sets 1 and 2. The nonuniform size of water droplets (Fig. 4(b)) tends to make a heterogeneous water network in comparison with the uniform size droplets (Fig. 4(a)). Fig. 5(a) shows the relative diffusivity for Sets 1 and 2. The relative diffusivity D_{r} decreases almost linearly in proportion to the water saturation S_{w}. Fig. 5(b) shows the dimensionless permeability for Sets 1 and 2. The dimensionless permeability K_{dl} decreases nonlinearly in proportion to the water saturation

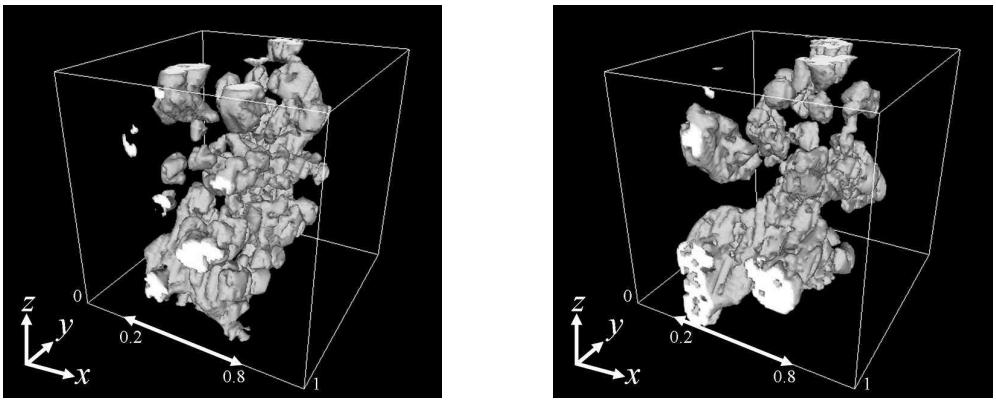

(a) (b)

Figure 4: Equilibrium configuration of water droplets, $S_w = 20\%$, (a) Set 1: $R = 16 \sim 24\mu$m and (b) Set 2: $R = 16 \sim 40\mu$m.

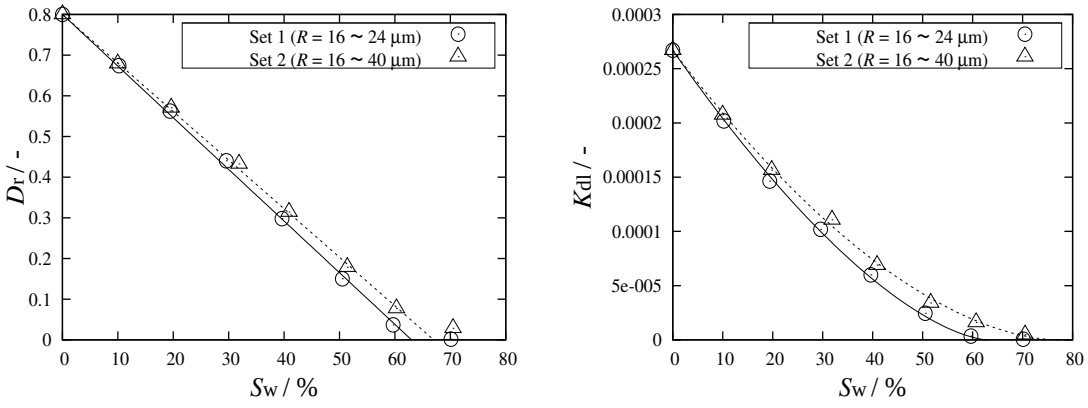

(a) (b)

Figure 5: (a) Relative diffusivity and (b) dimensionless permeability of Sets 1 and 2.

S_w. It is found from Fig. 5 that the heterogeneous water network (Set 2) improves both the diffusivity and the permeability.

4.2 The effect of porosity of GDL (Sets 1, 3 and 4)

Fig. 6 shows the configuration of water droplets for Sets 3 and 4. In the high porosity structure (Fig. 6(a)), the water network disperses and the void space for gas transport is kept. On the contrary, in the low porosity structure (Fig. 6(b)), the water network forms a membrane. Fig. 7(a) shows the relative diffusivity for Sets 3 and 4, and Fig. 7(b) shows the dimensionless permeability for Sets 3 and 4. In Fig. 7, the results of Set 1 are also shown for comparison. It is found from Fig. 7 that while the high porosity structure (Set 3) improves both the relative diffusivity D_r and the dimensionless permeability K_{dl},

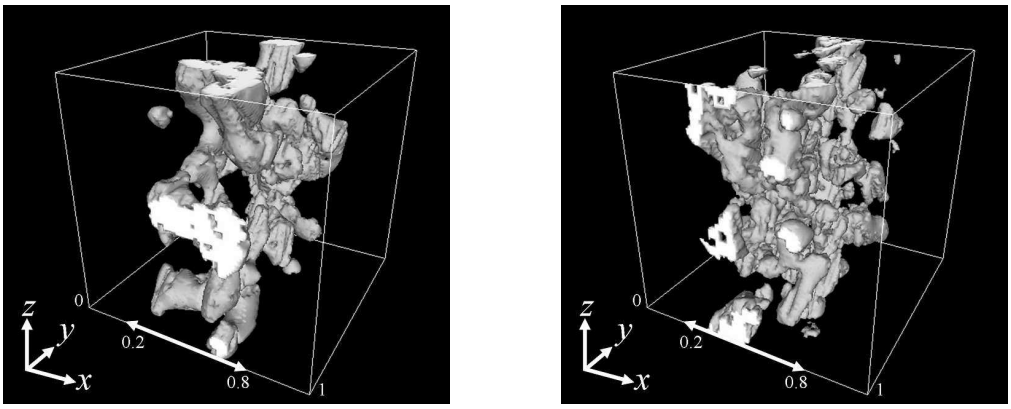

Figure 6: Equilibrium configuration of water droplets, $S_w = 20\%$, (a) Set 3 : $\epsilon = 86\%$ and (b) Set 4 : $\epsilon = 75\%$.

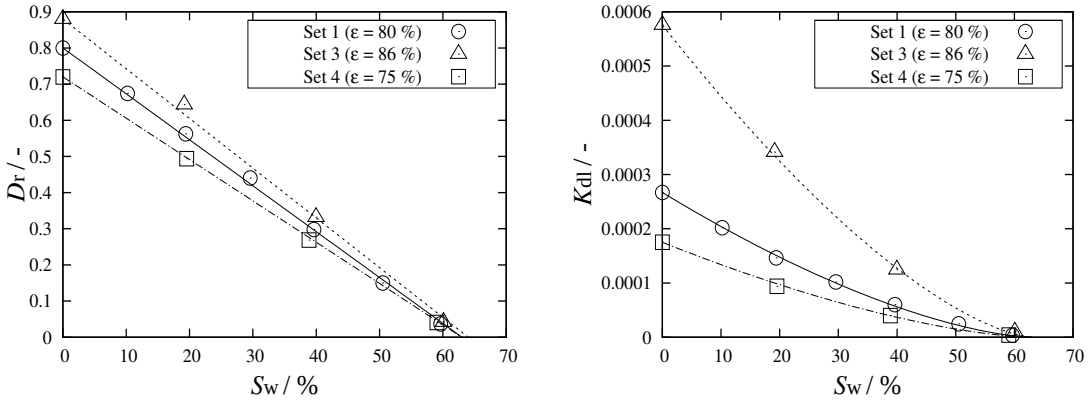

Figure 7: (a) Relative diffusivity and (b) dimensionless permeability of Sets 1, 3 and 4.

both values are decreased in the low porosity structure (Set 4). These results are quite reasonable, because the porosity directly relates the volume of the gas transport path.

4.3 The effect of viscosity ratio (Sets 1, 5 and 6)

Fig. 8 shows the configuration of water droplets for Sets 5 and 6. Although the viscosity ratio of water to air is changed, there is no significant difference between the two water configurations in Fig. 8. The relative diffusivity D_r and the dimensionless permeability K_{dl} are shown in Fig. 9. It is found that the viscosity ratio does not affect both the relative diffusivity D_r and the dimensionless permeability K_{dl}. The results indicates that the water configuration is not affected by the viscosity ratio of water to air, though the viscosity relates to the dynamics of water.

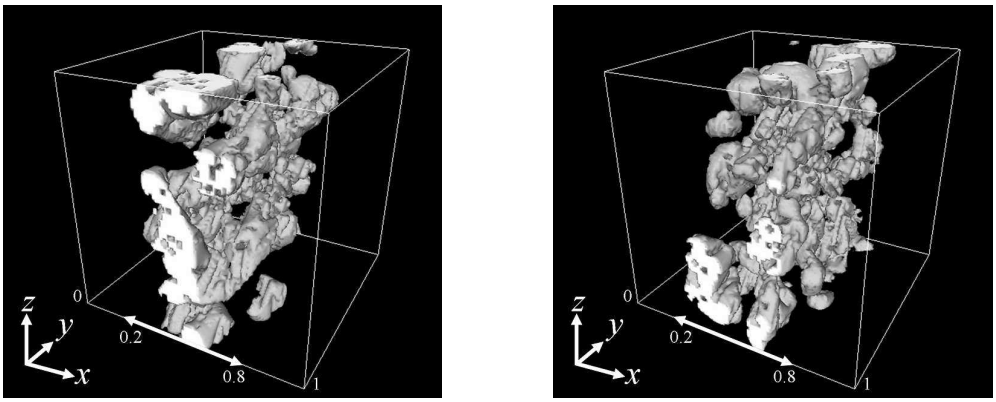

(a) (b)

Figure 8: Equilibrium configuration of water droplets, $S_w = 20\%$, (a) Set 5 : $M = 15$ and (b) Set 6 : $M = 100$.

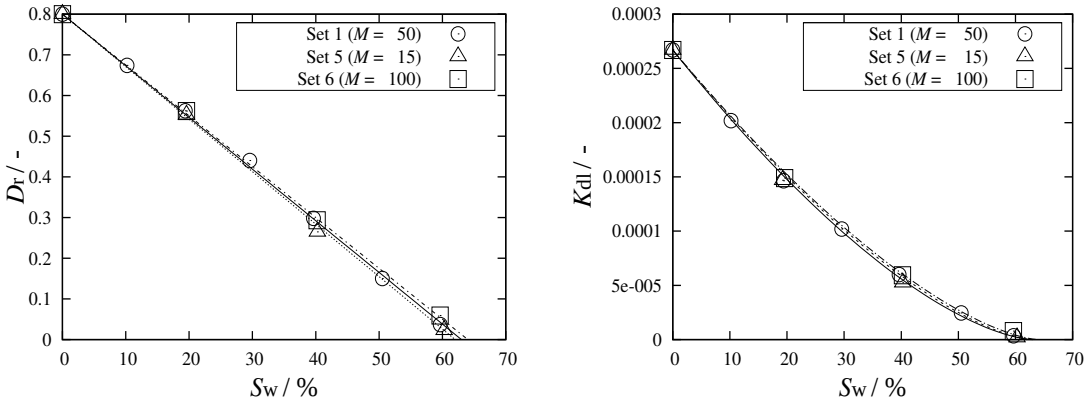

(a) (b)

Figure 9: (a) Relative diffusivity and (b) dimensionless permeability of Sets 1, 5 and 6.

4.4 The effect of wettability (Sets 1, 7 and 8)

Fig. 10 shows the configuration of water droplets for Sets 7 and 8. Since the surface of the fibers is hydrophobic, the water droplets are detached from the fibers and they become round. The relative diffusivity D_r and the dimensionless permeability K_{dl} are shown in Fig. 11. At the hydrophobic surface condition, the dimensionless permeability decreases, but the relative diffusivity does not change.

In order to explain the reason why the permeability decreases under the hydrophobic surface condition, the pore size distribution [17] of the GDL with the equilibrium configuration of water droplets is calculated. Fig. 12 shows the pore size distribution of Sets 1 and 8. While the pores are distributed in wide range of diameters in the case of the neutral surface (Set 1), the relatively small pores exist in the case of the hydrophobic surface (Set 8). On the hydrophobic surface, the water meets with the resistance of capillary force

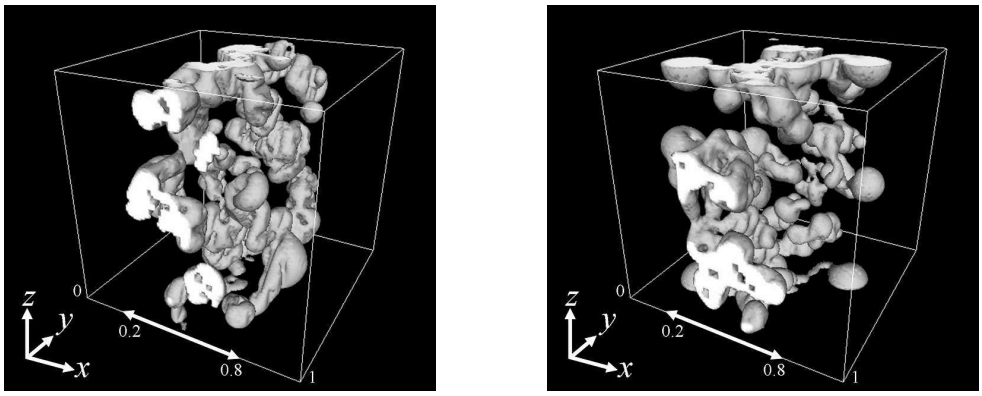

Figure 10: Equilibrium configuration of water droplets, (a) Set 7: $S_w = 20\%$, $\theta = 120^\circ$ and (b) Set 8: $S_w = 17\%$, $\theta = 150^\circ$.

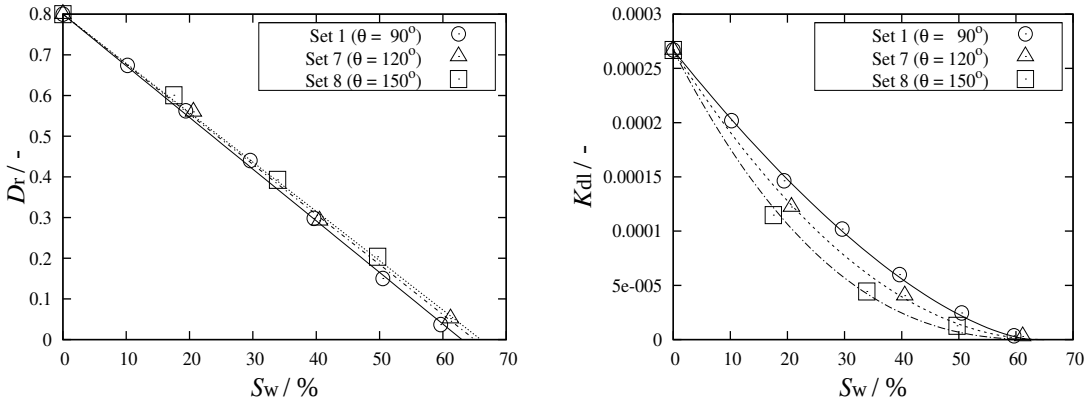

Figure 11: (a) Relative diffusivity and (b) dimensionless permeability of Sets 1, 7 and 8.

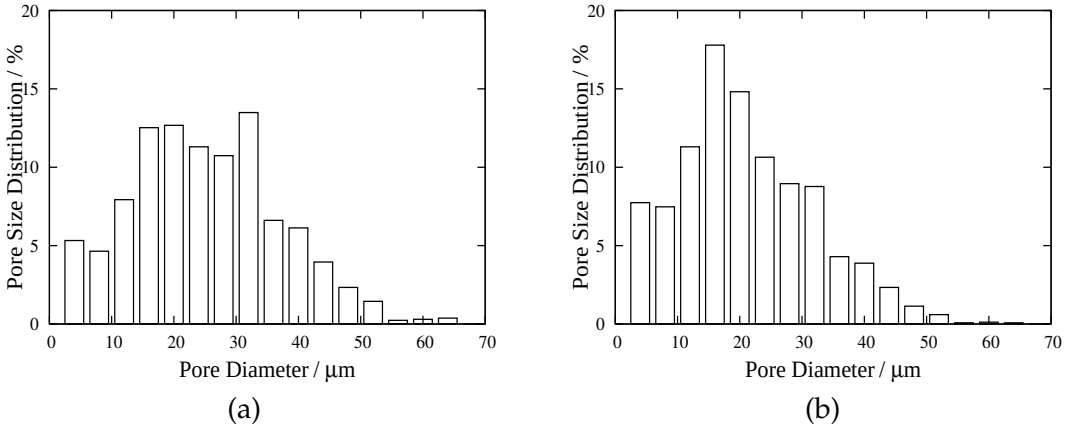

Figure 12: Pore size distribution, (a) Set 1: $S_w = 20\%$, $\theta = 90^\circ$ and (b) Set 8: $S_w = 17\%$, $\theta = 150^\circ$.

that is inversely proportional to the pore diameter, and thus the water moves from small pores to large pores to minimize the resistance. When the small pores are left for gas transport, the pressure drop becomes large. As a result, the permeability decreases. In contrast, the diffusivity does not decrease, because the volume of the gas transport path is kept even on the hydrophobic surface.

5 Conclusions

In this study, the lattice Boltzmann method has been applied to the investigation of the effects on the diffusivity and the permeability in the GDL of the PEFC operating conditions such as the configuration of water droplets, the porosity of the GDL, the viscosity ratio of water to air, and the surface wettability of the GDL. The following results are obtained:

- Since the high water saturation decreases the diffusivity and the permeability without exception, the low water saturation is desirable.
- The heterogeneous water network and the high porosity improve the diffusivity and the permeability.
- The viscosity ratio does not affect not only the configuration of water droplets, but also the diffusivity and the permeability in the GDL.
- The hydrophobic surface of the GDL affects the configuration of water droplets. As a result the permeability decreases, but the diffusivity does not change.

References

[1] M. Mathias, J. Roth, J. Fleming, and W. Lehnert, Diffusion Media Materials and Characterisation, Handbook of Fuel Cells-Fundamentals, Technology and Applications, John Wiley & sons, Ltd., 2003.
[2] J. A. Ramírez, S. N. Mendoza, and J. G. Trejo, Calculation of the effective diffusivity of heterogeneous media using the lattice-Boltzmann method, Phys. Rev. E., 53 (1996), 2298–2303.
[3] C. Pan, L. S. Luo, and C. T. Miller, An evaluation of lattice Boltzmann schemes for porous medium flow simulation, Comput. Fluids., 35 (2006), 898–909.
[4] J. H. Nam, and M. Kaviany, Effective diffusivity and water-saturation distribution in sigle- and two-layer PEMFC diffusion medium, Int. J. Heat. Mass. Trans., 46 (2003), 4595–4611.
[5] T. Munekata, T. Inamuro, and S. Hyodo, On the applicability of the Leverett function to capillary pressure: a lattice Boltzmann study, JSME B., 75 (2009), 1568–1575.
[6] K. Kobayashi, T. Inamuro, and F. Ogino, Numerical simulation of advancing interface in a micro heterogeneous channel by the lattice Boltzmann method, J. Chem. Eng. Jap., 39 (2006), 257–266.
[7] T. Inamuro, Lattice Boltzmann methods for viscous fluid flows and for two-phase fluid flows, Fluid. Dyn. Res., 38 (2006), 641–659.
[8] T. Lee, and C. L. Lin, A stable discretization of the lattice Boltzmann equation for simulation of incompressible two-phase flows at high density ratio, J. Comput. Phys., 206 (2005), 16–47.

[9] X. Shan, and H. Chen, Lattice Boltzmann model for simulating flows with multiple phase and components, Phys. Rev. E., 47 (1993), 1815–1819.
[10] J. Bear, Dynamics of Fluids in Porous Media, Dover Publications, Inc.,1972.
[11] D. d'Humières, I. Ginzburg, M. Krafczyk, P. Lallemand, and L. S. Luo, Multiple-relaxation-time lattice Boltzmann models in three dimensions, Phil. Trans. R. Soc. Lond. A., 360 (2002), 437–451.
[12] I. Ginzburg, and D. d'Humières, Multireflection boundary conditions for lattice Boltzmann models, Phys. Rev. E., 68 (2003), 066614.
[13] Q. Zou, S. Hou, S. Chen, and G. D. Doolen, An improved incompressible lattice Boltzmann model for time-independent flows, J. Stat. Phys., 81 (1995), 35–48.
[14] M. Bouzidi, M. Firdaouss, and P. Lallemand, Momentum transfer of a Boltzmann-lattice fluid with boundaries, Phys. Fluids., 13 (2001), 3452–3459.
[15] Q. Zou, and X. He, On pressure and velocity boundary conditions for the lattice Boltzmann model, Phys. Fluids., 9 (1997), 1591–1598.
[16] M. Yoshino, and T. Inamuro, Lattice Boltzmann simulations for flow and heat/mass transfer problems in a three-dimensional porous structure, Int. J. Numer. Methods. Fluids., 43 (2003), 183–198.
[17] L. D. Gelb, and K. K. Gubbins, Pore size distributions in porous glasses: a computer simulation study, Langmuir., 15 (1999), 305–308.